

High-pressure phase transitions of nitinol NiTi to a semiconductor with an unusual topological structure

HPSTAR
580-2018

Guangtao Liu,¹ Hanyu Liu,² Xiaolei Feng,³ and Simon A. T. Redfern^{3,4,*}¹National Key Laboratory of Shock Wave and Detonation Physics, Institute of Fluid Physics, China Academy of Engineering Physics, Mianyang 621900, China²Geophysical Laboratory, Carnegie Institution of Washington, Washington, DC 20015, USA³Department of Earth Sciences, University of Cambridge, Downing Street, Cambridge CB2 3EQ, United Kingdom⁴Center for High Pressure Science and Technology Advanced Research, Shanghai 201203, China

(Received 23 October 2017; revised manuscript received 5 January 2018; published 26 April 2018)

Systematic *ab initio* structure simulations have been used to explore the high-pressure behavior of nitinol (NiTi) at zero temperature. Our crystal structure prediction and first-principles calculations reveal that the known *B19* phase is dynamically unstable, and an orthorhombic structure (*Pbcm*) and a face-centered-cubic *B32* structure (*Fd $\bar{3}m$*) become stable above ~ 4 and 29 GPa, respectively. The predicted, highest-pressure, *B32* phase is composed of two interpenetrating diamond structures, with a structural topology that is quite distinct from that of the other phases of NiTi. Interestingly, the *B32* phase shows an unusual semiconducting characteristic as a result of its unique band structure and the nature of *3d* orbitals localization, whose expected synthesis pressure is accessible to current experimental techniques.

DOI: [10.1103/PhysRevB.97.140104](https://doi.org/10.1103/PhysRevB.97.140104)

I. INTRODUCTION

Nickel titanium (NiTi), termed nitinol, is widely used in automotive, aerospace, electronics, and mechanical engineering as well as in medical devices. It is well known for its shape memory and superelastic properties. Its shape memory behavior is driven by a reversible martensitic phase transition from a high-temperature austenitic *B2* (*Pm $\bar{3}m$*) phase into a low-temperature martensitic phase [1,2] at around 273 K. Experimentally, single crystal x-ray diffraction [3,4] and powder neutron diffraction measurements [5] have determined the low-temperature phase as *B19'* (*P2₁/m*) with $\gamma \sim 97.8^\circ$. Several experimental investigations have, however, reported the existence of multiple coexisting phases [6–8]. A large number of computational studies have been performed to uncover the underlying mechanism of phase transitions in NiTi [9–16]. *Ab initio* calculations revealed an additional orthorhombic *B19* (*Pmma*) phase as well as an “*R* phase” (*P3*), which are both low-symmetry distortions of the high-symmetry *B2* structure [17]. Density functional theory (DFT) calculations, in particular, have illuminated and explained the controversies about the energy surface and properties of NiTi, and have suggested results which are not always in agreement with the experimental observations. For example, the phonon frequencies of the experimentally observed ambient *B2* phase were calculated to be imaginary in conventional *ab initio* calculation, indicating that this structure is dynamically unstable [18]. Moreover, the experimentally observed low-temperature *B19'* structure was predicted to be unstable with respect to a higher-symmetry base-centered orthorhombic (BCO) *B33* (*Cmcm*) structure at zero temperature [17]; this *B33* structure has not yet been confirmed in any experimental study; furthermore, this

space group precludes this phase from being a shape memory martensite alloy derived from the cubic structure. Many of these differences can be resolved if temperature-dependent entropic effects are taken into account in the calculations. For example, a recent theoretical study has showed that *B2* and *B19'* structures are indeed stabilized, whereas the *B33* structure is destabilized at finite temperature [19].

Obviously, the temperature factor plays a significant role in the martensitic structural phase transition of NiTi, leading to its shape memory effect, as underlined in both experimental and theoretical studies. But in addition to temperature, pressure also plays a controlling role in inducing such transitions by altering the crystal and/or electronic structures and generally pressure is well recognized for creating novel structures and properties in materials, including metals and alloys. For example, a pressure-induced metal-semiconductor transition in lithium has been observed by direct electrical resistance measurements [20]. Transparent sodium was predicted by computational work, and then experimentally observed at high pressure, associated with pressure-induced *p-d* hybridization of valence electrons and their repulsion by core electrons into interstitial sites in the structure [21]. Further examples of pressure-induced structural transitions include that from disordered structure to a long-range face-centered-cubic (fcc) topological ordered structure in $\text{Ce}_{75}\text{Al}_{25}$, which was observed at 25 GPa [22]. The ground-state phase of the prototype CoCrFeMnNi high-entropy alloy was retained during a high-pressure irreversible phase transition under compression [23]. Nowadays, pressure has been recognized and deployed as a very powerful and useful technique in the design, exploration, and synthesis of novel functional materials. Following this path, the high-pressure properties and phase diagram of NiTi has been investigated using self-consistent *ab initio* lattice dynamical calculations which suggested that the *B19'* and *B19* structures are stable high-pressure phases [24].

*Corresponding author: satr@cam.ac.uk

In this work, we employ crystal structure predictions and first-principles total energy calculations based on DFT, to further explore the high-pressure behavior of NiTi at zero temperature. Here, we find that the known $B19$ phase is dynamically unstable and report that the ground-state $B33$ phase transforms into a $Pbcm$ phase at ~ 4 GPa, and finally to a $B32$ ($Fd\bar{3}m$) phase at ~ 29 GPa. Actually, we find that the predicted $Pbcm$ phase is a distorted structure derived from the dynamically unstable $B19$ phase. The uncovered $B32$ phase has a diamondlike stacking sequence, whose topological crystal structure is different from the structural configuration of NiTi. The more intriguing prediction that the high-pressure $B32$ phase is a semiconductor with a narrow direct band gap of ~ 0.26 eV, is a consequence of the special band structure associated with its unusual structural topology, which appears to be characterized by more localized $3d$ orbitals. Our findings indicate that metallic NiTi alloy displays a rich family of abundant structural phase transitions and will transform into an interesting semiconducting state at high pressure, appearing to show a different class of physical and chemical mechanisms of transformation for transition-metal alloys.

II. COMPUTATIONAL DETAILS

The crystal structures of NiTi were probed systematically using the crystal structure analysis by particle swarm optimization (CALYPSO) code [25,26], which is based on a search for the global minimum in the free-energy surfaces computed by the DFT total energy calculations. This method has been applied successfully to a wide range of crystalline systems ranging from elemental solids to binary and ternary compounds [27–30]. The simulation cell comprised 1–8 f.u. (2–16 atoms) of NiTi at 0, 10, and 40 GPa. The population size of each generation was 50. The best 20 structures from last generation and 30 new ones generated by the CALYPSO algorithm composed the next generation. Generally, the search was terminated after the generation of 2000–2500 structures.

DFT calculations, including structural optimizations, enthalpies, electronic structures, and phonons, were performed using the Vienna *ab initio* simulation package (VASP) [31] code employing the Perdew-Burke-Ernzerhof [32] exchange-correlation functional. The $3d^8 4s^2$ and $3d^2 3s^2$ electrons were treated as valence electrons for Ni and Ti, respectively. Usually, the parameters of the structure searching are a little coarser than those of normal optimizations and enthalpy calculations to save CPU time, where energy cutoff is 400 eV and the Monkhorst-Pack grid is $2\pi \times 0.05 \text{ \AA}^{-1}$ in reciprocal space here. We selected a lot of candidates (20–50) with low energy, then reoptimized all of them more precisely. To ensure that all enthalpy calculations were well converged, to about 1 meV/atom, a Monkhorst-Pack grid was selected with sufficient density ($2\pi \times 0.05 \text{ \AA}^{-1}$) in reciprocal space, as well as appropriate energy cutoff (450 eV) [33].

The phonon calculations and modulation of soft phonon mode were carried out using a finite displacement approach [34] through the PHONOPY code [35], which uses the Hellmann-Feynman forces calculated from the optimized supercells through the VASP code. In our calculations of phonon spectra, we selected $2\pi \times 0.04 \text{ \AA}^{-1}$ and 700 eV as the parameters and

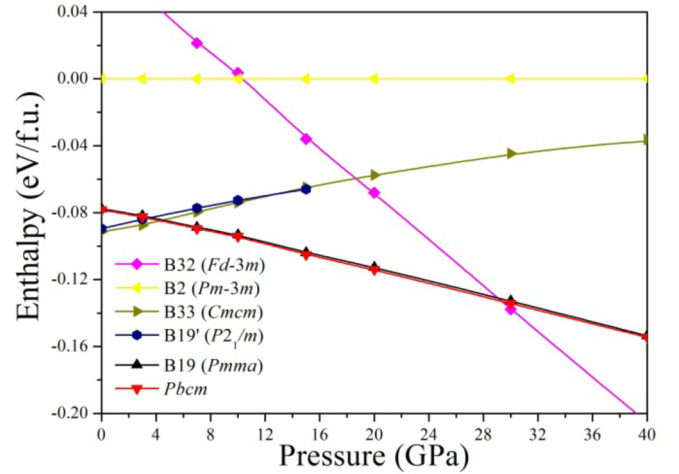


FIG. 1. The calculated enthalpy as a function of pressure for each NiTi structure.

extended the unit cells to be big enough supercells with volume larger than $\sim 1000 \text{ \AA}^3$. For the $B19$ structure, the supercell is $3 \times 4 \times 3$, including 144 atoms; for the $Pbcm$ structure, the supercell is $3 \times 4 \times 1$, including 96 atoms; and for the $B32$ structure, the supercell is $2 \times 2 \times 2$, including 128 atoms.

III. RESULTS AND DISCUSSION

To validate our computational prediction method and DFT calculations in the NiTi system, using the CALYPSO search, we successfully reproduced the known ambient $B2$ phase, low-temperature $B19'$ phase, and the ground-state (0 K) $B33$ phase at atmospheric pressure, as well as their energy ordering, $H(B2) > H(B19') > H(B33)$, verifying the reliability of our methodology. Then an orthorhombic $Pbcm$ phase and another cubic $B32$ phase were found during structure searching at 10 and 40 GPa, respectively. The enthalpy of each phase as a function of pressure is indicated in Fig. 1. We find that the enthalpy of the $B33$ phase is just a little lower than that of the $B19'$ phase, which is consistent with previous studies [19]. The $B33$ phase is stable up to ~ 4 GPa, then transforms to the $B19$ phase or the $Pbcm$ phase. It can be seen that it is very difficult to distinguish them on the basis of their energy, because the energy difference between these two primitive orthorhombic structures is less than the convergence accuracy of the energy calculation. At higher pressure (29 GPa), the $B32$ phase becomes enthalpically favored.

In addition to the enthalpy calculations for these structures, we have also calculated their phonon dispersion curves. The dynamic stabilities of the $B33$ phase and $B19'$ phase have been confirmed in theoretical study previously [19]. For the $B19$ phase, we found a soft phonon branch with negative frequencies running from the Γ point (0,0,0) to the Z point (0,0,0.5) to the T point ($-0.5, 0, 0.5$) of the Brillouin zone (BZ) indicating that this structure is dynamically unstable [Fig. 2(a)]. We therefore modulated the structure by introducing atomic displacements corresponding to the wave vector of the Z point within a supercell of the $B19$ structure and we obtained a $Pbcm$ structure, which is the same structure as obtained in our crystal structure predictions. Actually, the crystal structure of the predicted $Pbcm$ phase is a distorted

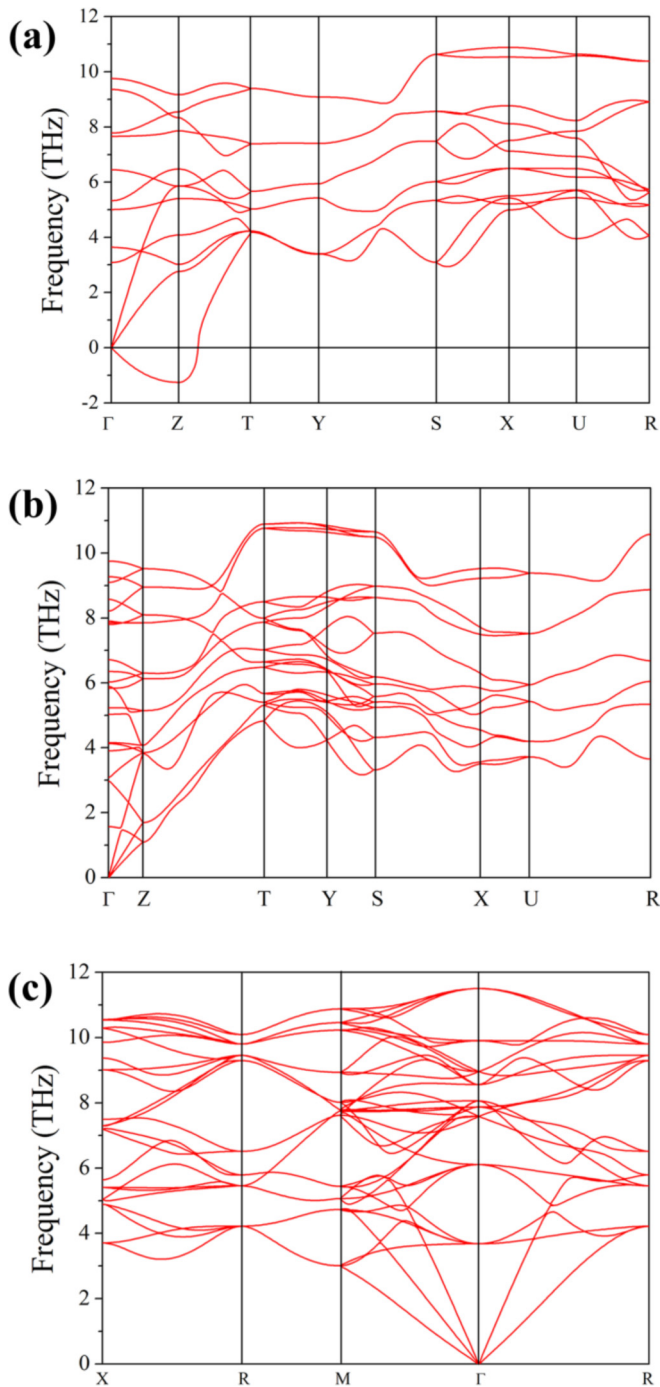


FIG. 2. The phonon dispersions of NiTi in its (a) $B19$ structure at 20 GPa, (b) $Pbcm$ structure at 20 GPa, and (c) $B32$ structure at 40 GPa.

supercell of the known $B19$ phase. Over the entire BZ, we found no imaginary phonon frequencies for this $Pbcm$ phase or for the $B32$ phase, confirming the dynamic stability of each of these two structures [Figs. 2(b) and 2(c)]. We also confirmed their mechanical stabilities by computing the elastic constants [33]. Therefore, by considering both thermal and dynamical stabilities, it appears safe to conclude that, at zero temperature, the $Pbcm$ phase and the $B32$ phase are calculated to be stable above ~ 4 and ~ 29 GPa, respectively.

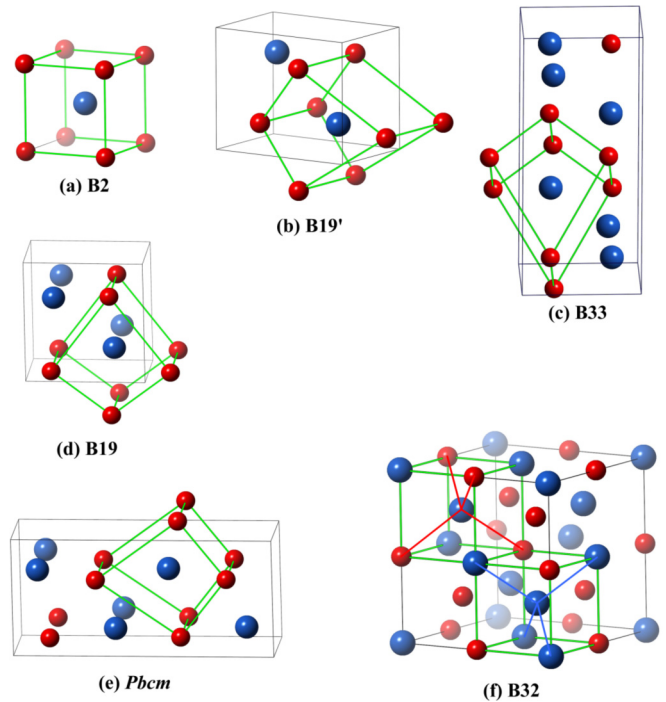


FIG. 3. The schematic crystal structures of the NiTi phases (a) $B2$, (b) $B19'$, (c) $B33$, (d) $B19$, (e) $Pbcm$, and (f) $B32$. Large blue and small red spheres represent Ni and Ti atoms, respectively.

In order to better understand the nature of the phase transitions between the high-pressure polymorphs of NiTi, we consider the crystal structures and details of these phases, as shown in Fig. 3 and Table I. Careful observation of these NiTi crystal structures reveals that all of them, except the $B32$ phase, share the same structural topology. They can all be derived from the highly symmetric simple cubic $B2$ structure. In these phases, each Ti atom is eightfold coordinated by Ni atoms and then regular or irregular hexahedra form their crystal structures. Both the temperature-induced martensitic phase transition ($B2 \rightarrow B19'$) and our pressure-induced phase transition ($B33 \rightarrow Pbcm$) can be seen in terms of the varying relative displacements of Ni and Ti atoms, derived from a (seriously) distorted $B2$ structure.

In contrast, the high-pressure $B32$ structure shows a completely different topological crystal structure, and can be viewed as two interpenetrating diamond structures separated by a vector of $(0.5, 0.5, 0.5)$. Each Ti atom is tetrahedrally coordinated by four Ti atoms and by four Ni atoms at identical distances, thus forming a superstructure of the body-centered-cubic (bcc) lattice, which often occurs in certain intermetallic I-III compounds (LiAl, LiGa, NaTl) and I-IIIB alloys (LiZn, LiCd) [36]. Thus, it can be seen that the transformation to the $B32$ phase involves a significant topological rearrangement and is a reconstructive phase transition, in contrast with the other structural phase transitions in NiTi. Therefore, the energy barrier of reconstructive phase transition ($Pbcm \rightarrow B32$) is expected to be significantly higher than that of the lower-pressure transition ($B33 \rightarrow Pbcm$). Additionally, we have calculated the equation of states of all these NiTi structures [33]. We find that the $B32$ phase is significantly denser than the other phases due to the

TABLE I. The calculated crystal structure information of NiTi at different pressures.

Space group	Pressure (GPa)	Lattice parameters (Å)	Atoms	x	y	z
$Pm\bar{3}m(B2)$	0	$a = 3.003$	Ti	0.5	0.5	0.5
			Ni	0	0	0
$P2_1/m(B19')$	0	$a = 4.687$	Ti	0.2189	0.25	0.0127
		$b = 4.038$	Ni	0.6746	0.25	0.0491
		$c = 2.930$				
		$\beta = 98.97^\circ$				
$Cmcm(B33/BCO)$	0	$a = 2.888$	Ti	0	0.1440	0.75
		$b = 9.398$	Ni	0	0.5847	0.25
		$c = 4.042$				
$Pmma(B19)$	20	$a = 4.176$	Ti	0.25	0	0.2923
		$b = 2.578$	Ni	0.25	0.5	0.8172
		$c = 4.505$				
$Pbcm$	20	$a = 2.572$	Ti	0.0528	0.3975	0.25
		$b = 9.029$	Ni	0.5357	0.1598	0.25
		$c = 4.176$				
$Fd\bar{3}m(B32)$	40	$a = 5.585$	Ti	0.5	0.5	0
			Ni	0	0	0.5

nature change from (distorted) bcc stacking to a close-packed fcc one, further underlining the expectation that this phase becomes most stable at extreme pressure.

To further investigate the electronic properties of NiTi, the band structures and the density of states (DOS) of all phases were studied by first-principles calculations. It is expected that the $B2$, $B33$, and $Pbcm$ phases show metallic behavior, as in a typical alloy system, where the valence bands and conduction bands completely overlap and the DOS at the Fermi level is very high [33]. However, our computational results indicate that the predicted $B32$ structure shows a band gap. It is well known that DFT usually underestimates the band gap of materials, and we thus employed the screened hybrid functional of Heyd, Scuseria, and Ernzerhof (HSE06) [37] to better determine the electronic properties of this structure. The modified band structure (Fig. 4) clearly shows that the $B32$ phase shows semiconducting character with a direct band gap of ~ 0.26 eV between the Γ and X points, which is consistent

with its DOS. From the projected DOS, we find that most of the electronic states below the Fermi level are associated with Ni $3d$ electrons, but also partly by Ti $3d$ electrons and their s , p orbitals. In contrast, the conduction band is composed mainly of Ti $3d$ electrons.

Here, the electronic properties of the $B32$ phase may directly contribute to the nature of its crystal structure, a Zintl phase. Usually, such structures are poor conductors or semiconductors. Normally, such phases are the products of a reaction between group I/III elements and any post-transition metal or metalloid. The classic Zintl phase, NaTl, displays complete electron transfer from the more electropositive Na to the more electronegative Tl, just as in genuine ionic salts such as NaCl [38]. It behaves like a group-IV element, and it forms a diamond network structure. Thus, the band structure and density of states have characteristics related to those of the tetrahedrally bonded IV-IV semiconductors. For example, a study of LiAl indicates that while the Li-Al bond is an ionically

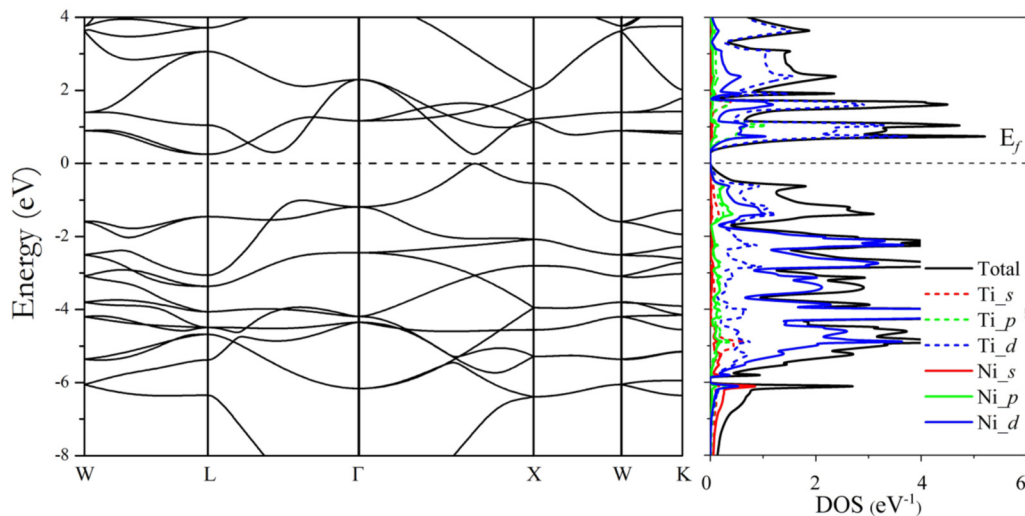


FIG. 4. Band structure along the high-symmetry path and the projected DOS of the $B32$ structure at 40 GPa. The Fermi level has been set to 0 eV.

polarized covalent bond, the Al-Al bonds are metalliclike and the Li-Li interactions are essentially nonbonding. It was found that this system shows a semimetallic band structure [39]. Our Bader population analysis [40] reveals an electron transfer of $\sim 0.88e$ from Ti to Ni in the *B32* phase. In this *B32* phase Ti and Ni show, to first approximation, +1 and -1 valence states, respectively, akin to LiAl, and the *B32* structure of NiTi shows an obvious band gap.

IV. CONCLUSIONS

In summary, we performed systematically theoretical studies on the structural variability and associated physical properties of NiTi alloy at high pressures. Through structure prediction method and first-principles calculations, at zero temperature, we identify that its ground-state *B33* phase transforms into a predicted higher-pressure *Pbcm* phase, and then to a highly symmetric *B32* phase under increased compression. Further DFT studies reveal that the uncovered *B32* phase of this

NiTi alloy shows an interestingly semiconducting behavior, which is associated with its special topological phase transition and the characteristic of *3d* electrons. The present study provides insights into the exploration and design of distinctive alloy materials under extreme conditions.

ACKNOWLEDGMENTS

The authors acknowledge funding support from the National Natural Science Foundation of China under Grant No. 11604314. Work at Carnegie was supported by Energy Frontier Research in Extreme Environments Center (EFree), an Energy Frontier Research Center funded by the Department of Energy (DOE), Office of Science, Basic Energy Sciences under Award No. DE-SC-0001057. S.A.T.R. acknowledges the support of the UK Natural Environment Research Council under Grant No. NE/P012167/1. X.L.F. is grateful for the support of the China Scholarship Council.

- [1] J. A. Shaw and S. Kyriakides, *J. Mech. Phys. Solids* **43**, 1243 (1995).
- [2] O. Benafan, S. A. Padula II, R. D. Noebe, T. A. Sisneros, and R. Vaidyanathan, *J. Appl. Phys.* **112**, 093510 (2012).
- [3] Y. Kudoh, M. Tokonami, and K. Otsuka, *Acta Metall.* **33**, 2049 (1985).
- [4] G. M. Michal and R. Sinclair, *Acta Crystallogr., Sect. B: Struct. Crystallogr. Cryst. Chem.* **37**, 1803 (1981).
- [5] H. Search, C. Journals, A. Contact, M. Iopscience, and I. P. Address, *J. Phys. F: Met. Phys.* **13**, L77 (1983).
- [6] P. Taylor, M. J. Marcinkowski, A. S. Sastri, and D. Koskimaki, *Philos. Mag.* **18**, 945 (1968).
- [7] J. M. Carpenter, *Acta Metall. Mater.* **38**, 1291 (1990).
- [8] F. E. Wang, S. J. Pickart, and H. A. Alperin, *J. Appl. Phys.* **43**, 97 (1972).
- [9] J. Wang and H. Sehitoglu, *Appl. Phys. Lett.* **101**, 081907 (2012).
- [10] A. Pasturel, C. Colinet, D. N. Manh, A. T. Paxton, and M. van Schilfgaarde, *Phys. Rev. B* **52**, 15176 (1995).
- [11] X. Huang, C. Bungaro, V. Godlevsky, and K. M. Rabe, *Phys. Rev. B* **65**, 014108 (2001).
- [12] X. Wang, *Phys. Rev. B* **78**, 092103 (2008).
- [13] N. Hatcher, O. Y. Kontsevoi, and A. J. Freeman, *Phys. Rev. B* **80**, 144203 (2009).
- [14] N. Hatcher, O. Y. Kontsevoi, and A. J. Freeman, *Phys. Rev. B* **79**, 020202 (2009).
- [15] D. Holec, M. Friak, A. Dlouhy, and J. Neugebauer, *Phys. Rev. B* **84**, 224119 (2011).
- [16] K. Guda Vishnu and A. Strachan, *Phys. Rev. B* **85**, 014114 (2012).
- [17] X. Huang, G. J. Ackland, and K. M. Rabe, *Nat. Mater.* **2**, 307 (2003).
- [18] K. Parlinski and M. Parlinska-Wojtan, *Phys. Rev. B* **66**, 064307 (2002).
- [19] J. B. Haskins, A. E. Thompson, and J. W. Lawson, *Phys. Rev. B* **94**, 214110 (2016).
- [20] T. Matsuoka and K. Shimizu, *Nature (London)* **458**, 186 (2009).
- [21] Y. Ma, M. Eremets, A. R. Oganov, Y. Xie, I. Trojan, S. Medvedev, A. O. Lyakhov, M. Valle, and V. Prakapenka, *Nature (London)* **458**, 182 (2009).
- [22] Q. S. Zeng, H. Sheng, Y. Ding, L. Wang, W. Yang, J.-Z. Jiang, W. L. Mao, and H.-K. Mao, *Science*. **332**, 1404 (2012).
- [23] F. Zhang, Y. Wu, H. Lou, Z. Zeng, V. B. Prakapenka, E. Greenberg, Y. Ren, J. Yan, J. S. Okasinski, X. Liu, Y. Liu, Q. Zeng, and Z. Lu, *Nat. Commun.* **8**, 1 (2017).
- [24] C. Hu, Z. Zeng, Z. Niu, L. Cai, C. Kong, and Y. Cui, *J. Alloys Compd.* **608**, 258 (2014).
- [25] Y. Wang, J. Lv, L. Zhu, and Y. Ma, *Phys. Rev. B* **82**, 094116 (2010).
- [26] Y. Wang, J. Lv, L. Zhu, and Y. Ma, *Comput. Phys. Commun.* **183**, 2063 (2012).
- [27] J. Lv, Y. Wang, L. Zhu, and Y. Ma, *Phys. Rev. Lett.* **106**, 015503 (2011).
- [28] G. Liu, S. Besedin, A. Irodova, H. Liu, G. Gao, M. Eremets, X. Wang, and Y. Ma, *Phys. Rev. B* **95**, 104110 (2017).
- [29] M. Zhang, H. Liu, Q. Li, B. Gao, Y. Wang, H. Li, C. Chen, and Y. Ma, *Phys. Rev. Lett.* **114**, 015502 (2015).
- [30] Y. Li, J. Hao, H. Liu, S. Lu, and J. S. Tse, *Phys. Rev. Lett.* **115**, 105502 (2015).
- [31] G. Kresse and J. Furthmüller, *Phys. Rev. B* **54**, 11169 (1996).
- [32] J. P. Perdew, K. Burke, and M. Ernzerhof, *Phys. Rev. Lett.* **77**, 3865 (1996).
- [33] See Supplemental Material at <http://link.aps.org/supplemental/10.1103/PhysRevB.97.140104> for details of test for parameter convergence as well as the elastic constants, equations of state and band structures of all NiTi phases.
- [34] K. Parlinski, Z. Q. Li, and Y. Kawazoe, *Phys. Rev. Lett.* **78**, 4063 (1997).
- [35] A. Togo, F. Oba, and I. Tanaka, *Phys. Rev. B* **78**, 134106 (2008).
- [36] M. Tadin, J. Schneider, H. Boysen, and F. Frey, *Mater. Sci. Forum* **79-82**, 635 (1991).
- [37] J. Heyd, G. E. Scuseria, and M. Ernzerhof, *J. Chem. Phys.* **118**, 8207 (2003).
- [38] Sevov, S. C. Zintl Phases, *In Intermetallic Compounds-Principles and Practice*, edited by J. H. Westbrook, and R. L. Fleischer (John Wiley & Sons. Ltd.: Chichester, England, 2002), Vol. 3, pp. 113–132.
- [39] Z. Alex, *Phys. Rev. B* **17**, 2582 (1978).
- [40] W. Tang, E. Sanville, and G. Henkelman, *J. Phys.: Condens. Matter* **21**, 084204 (2009).